Supporting Information

Local Lattice Distortion-Driven Highly Efficient Luminescence and Thermal Quenching Resistance in Sb^{3+}-Doped Hybrid Indium Chlorides

*Qingyi liu,[a] Junliang Li,[a] Qi Zhang,[a] Dongfeng Xue, [b, c, d, *] Lizhen Zhang,[e] Yan Yu [a, *] and Lingyun Li,[a, d, *]*

[a] Key Laboratory of Advanced Materials Technologies, International (Hong Kong Macao and Taiwan) Joint Laboratory on Advanced Materials Technologies, College of Materials Science and Engineering, Fuzhou University, Fuzhou, 350108, P. R. China

[b] University of Electronic Science and Technology of China, Chengdu, 611731, P. R. China

[c] Shenzhen Institute for Advanced Study, University of Electronic Science and Technology of China, Shenzhen, 518110, P. R. China

[d] SIAS, UESTC-JIREOIMD Joint Institute of Rare Earth Optoelectronic Information Materials and Devices, Shenzhen 518110, P. R. China

[e] State Key Laboratory of Functional Crystals and Devices, Fujian Institute of Research on the Structure of Matter, Chinese Academy of Sciences, Fuzhou City, Fujian Province 350002, P. R. China

Contents

1. Experimental Section

1.1 Chemical reagents

Benzyl-dimethyl-phenylazanium chlorid ($C_{15}H_{18}NCl$, ≥ 98%), Indium (III) chloride tetrahydrate ($InCl_3$•$4H_2O$, 99%), Antimony acetate ($C_6H_9O_6Sb$, 97%) and Bismuth (III) chloride ($BiCl_3$, 98%) were purchased from Shanghai Macklin Biochemical Co. Ltd. Hydrochloric acid (HCl, 36 - 38% in H_2O) was purchased from Sinopharm Chemical Reagent Co. Ltd. All starting reagents were used without purification.

1.2 Synthesis methods

Synthesis of $(C_{15}H_{18}N)_2InCl_5$: Benzyl-dimethyl-phenylazanium chloride ($C_{15}H_{18}NCl$, 0.247 g, 1mmol) and Indium (III) chloride tetrahydrate ($InCl_3 \cdot 4H_2O$, 0.293 g, 1 mmol) were added to a 5 mL mixed solution composed of hydrochloric acid and ethanol at a volume ratio of 3:2. The mixture was stirred at 50 °C for 10 min., resulting in a pale yellow clear solution. Subsequently, the solvent was slowly evaporated at 50 °C for approximately 3 hours, and white crystals precipitated at the liquid surface. After being washed with ethanol, the obtained crystals were transferred to a drying oven maintained at 60 °C to further evaporate the solvent. The reaction yield was approximately 31.81%, based on In. Elemental analysis calcd (%): $(C_{15}H_{18}N)_2InCl_5$ (716.3), C 50.26, N 3.91, H 5.03; found, C 50.01, N 3.99, H 5.01.

Synthesis of $(C_{15}H_{18}N)_2In_{1-x}Sb_xCl_5$ *and* $(C_{15}H_{18}N)_2In_{1-x}Bi_xCl_5$: Crystals of Sb^{3+}-doped compound $(C_{15}H_{18}N)_2In_{1-x}Sb_xCl_5$ and Bi^{3+}-doped compound $(C_{15}H_{18}N)_2In_{1-x}Bi_xCl_5$ were synthesized following a procedure analogous to that described above. $C_6H_9O_6Sb$ and $BiCl_3$ were employed as the respective sources of Sb^{3+} and Bi^{3+} for the partial substitution of In^{3+}.

1.3 Single Crystal Structure Determination

The single crystals of $(C_{15}H_{18}N)_2InCl_5$ was chosen for indexing and crystal structure analysis. It was measured using XtaLAB Pro II AFC12 (RINC) that were fitted with a graphite-monochromated Mo Kα radiation (λ = 0.71073 Å) at 296 K and 170 K, respectively. The Rigaku CrystalClear (version 1.4) software package processed the area detector data and the collection of diffraction images. The intensity data were corrected for polarization effects, Lorentz, and semiempirical factors. The crystal structures were solved by direct methods and refined by full-matrix least-squares fitting on F2 using the SHELX-97 program package. All atoms were refined with anisotropic thermal parameters. The structure was also checked for possible missing symmetry with PLATON. Crystallographic data and structural refinements are summarized in **Table S1** - **S4**.

1.4 Characterization

Thermogravimetric analysis (TGA) data were recorded on a Thermal Analysis Instrument (STA449-F5 Jupiter, Netzsch, Germany) from room temperature to 800 °C with a heating rate of

10 °C/min under nitrogen atmosphere. The powder X-ray diffraction (PXRD) patterns were obtained on a Rigaku miniflex 600 instrument with Cu Kα (λ = 1.54184 Å) radiation for phase identification. The UV-Vis-NIR diffuse reflectance spectra (DRS) in a wavelength range of 200 - 800 nm were collected by Lambda 950 spectrophotometer (PerkinElmer Instruments), during which $BaSO_4$ was used for the reference. The Raman spectra were recorded in the range of 30 - 1070 cm^{-1} using a RMS1000 Raman Microscope (Edinburgh Instruments) with a 532 nm laser excitation wavelength. And the temperature-dependent Raman spectra measurement, the sample was placed on a THMS type heating table (Linkam Scientific Instruments) and excited by 532 nm laser.

1.5 Optical spectroscopy measurement

The photoluminescence (PL) properties including the emission and excitation spectra in solid state were measured on a FLS1000 fluorescence spectrometer (Edinburgh Instruments). The PLQY analysis was performed using the same light source with an additional integrating sphere. The dynamics of emission decay were monitored by using the FLS1000 time-correlated single-photon counting capability with data collection for 1000 counts. Microsecond lifetime measurement is achieved through excitation by a microsecond flash lamp, and nanosecond lifetime measurement by an Edinburgh EPL ps pulsed diode laser. For the temperature-dependent emission spectra measurement, the sample was placed on a THMS type heating table (Linkam Scientific Instruments) and excited by xenon lamp. The temperature-dependent emission spectra of the samples were measured in the temperature range of 80 - 300 K and 300 - 400 K, respectively. The spectral data of temperature sensing device is collected by BSHP (BAISI Optoelectronic) high performance optical fiber spectrometer.

1.6 DFT Calculations

All the first-principles were performed by using density functional theory (DFT), as implemented in the Vienna ab initio Simulation Package (VASP)[1]. The generalized gradient approximation (GGA)[2] with Perdew-Burke-Ernzerh (PBE)[3] form for the exchange-correlation functional was used. The kinetic energy cutoff of the plane-wave basis was set as 700 eV. And the Brillouin zones of the primitive cell were sampled with Monkhorst–Pack k-mesh of 3 × 4 × 5. All the geometric structures were fully relaxed until the residual forces on each atom were less than 10^{-4} eV/Å, and set 10^{-8} eV/ Å as the criterion of convergence for total energy. Considering the 0D crystal structure of compounds, the weak interactions were corrected by using the DFT-D3[4] dispersion correction. The phonon dispersions are calculated using VASP and PHONONPY[5] packages with 1 × 1 × 2 supercell. The corresponding numbers of k-mesh are accordingly scaled down compared with the case of primitive cell calculation. And the doped structure $(C_{15}H_{18}N)_2In_{1-x}Sb_xCl_5$ and $(C_{15}H_{18}N)_2In_{1-x}Bi_xCl_5$ is obtained by replacing one In^{3+} in the unit cell with Sb^{3+}or Bi^{3+}, which are convenient for calculation.

2. Supplementary Tables

Table S1. Crystal data and structure refinement for $(C_{15}H_{18}N)_2InCl_5$ at 296K

Compound	$(C_{15}H_{18}N)_2InCl_5$
Empirical formula	$C_{30}H_{36}Cl_5InN_2$
Formula weight	716.68
Temperature/K	296(2)
Crystal system	monoclinic
Space group	*C*2
a/Å	16.190(3)
b/Å	12.555(3)
c/Å	8.3675(16)
α/°	90
β/°	103.877(3)
γ/°	90
Volume/Å^3	1651.2(6)
Z	2
ρ_{calc}g/cm^3	1.441
μ/mm^{-1}	1.142
F(000)	728
Crystal size/mm^3	0.12 × 0.11 × 0.1
Radiation	MoK_α (λ = 0.71073)
2Θ range for data collection/°	4.152 to 50.006
Index ranges	$-19 \le h \le 19$, $-14 \le k \le 14$, $-9 \le l \le 9$
Reflections collected	4720
Independent reflections	2632 [R_{int} = 0.0148, R_{sigma} = 0.0270]
Data/restraints/parameters	2632/1/176
Goodness-of-fit on F^2	1.04
Final *R* indexes [I>=2σ (I)]	R_1 = 0.0142, wR_2 = 0.0346
Final *R* indexes [all data]	R_1 = 0.0142, wR_2 = 0.0346
Largest diff. peak/hole / e Å^{-3}	0.18/-0.19
Flack parameter	0.018(16)

Table S2. Bond Lengths for $(C_{15}H_{18}N)_2InCl_5$ at 296K

Atom	Atom	Length/Å	Atom	Atom	Length/Å
In_{00}	Cl_{02}	2.4059(11)	C_{007}	C_{008}	1.383(4)
In_{00}	Cl_{03}	2.5278(7)	C_{007}	C_{009}	1.371(4)
In_{00}	Cl_{03}^{1}	2.5278(7)	C_{008}	C_{00A}	1.378(5)
In_{00}	Cl_{04}^{1}	2.3981(9)	C_{009}	C_{00D}	1.379(6)
In_{00}	Cl_{04}	2.3981(9)	C_{00A}	C_{00I}	1.366(6)
N_{005}	C_{007}	1.496(4)	C_{00B}	C_{00H}	1.491(5)
N_{005}	C_{00B}	1.544(4)	C_{00D}	C_{00I}	1.374(7)
N_{005}	C_{00C}	1.494(4)	C_{00F}	C_{00G}	1.371(6)
N_{005}	C_{00E}	1.518(5)	C_{00F}	C_{00H}	1.381(5)
C_{006}	C_{00H}	1.402(6)	C_{00G}	C_{00K}	1.380(7)
C_{006}	C_{00J}	1.367(8)	C_{00J}	C_{00K}	1.365(8)

Table S3. Bond Angles for $(C_{15}H_{18}N)_2InCl_5$ at 296K

Atom	Atom	Atom	Angle/°	Atom	Atom	Atom	Angle/°
Cl_{02}	In_{00}	Cl_{03}	90.53(3)	C_{008}	C_{007}	N_{005}	118.2(2)
Cl_{02}	In_{00}	Cl_{03}^{1}	90.53(3)	C_{009}	C_{007}	N_{005}	120.9(3)
Cl_{03}	In_{00}	Cl_{03}^{1}	178.93(6)	C_{009}	C_{007}	C_{008}	120.9(3)
Cl_{04}^{1}	In_{00}	Cl_{02}	115.61(3)	C_{007}	C_{008}	C_{00A}	119.3(3)
Cl_{04}	In_{00}	Cl_{02}	115.61(3)	C_{007}	C_{009}	C_{00D}	118.7(3)
Cl_{04}^{1}	In_{00}	Cl_{03}	89.92(3)	C_{00I}	C_{00A}	C_{008}	120.3(3)
Cl_{04}^{1}	In_{00}	Cl_{03}^{1}	89.62(3)	C_{00H}	C_{00B}	N_{005}	113.7(3)
Cl_{04}	In_{00}	Cl_{03}	89.62(3)	C_{00I}	C_{00D}	C_{009}	121.0(4)
Cl_{04}	In_{00}	Cl_{03}^{1}	89.92(3)	C_{00G}	C_{00F}	C_{00H}	120.1(4)
Cl_{04}^{1}	In_{00}	Cl_{04}	128.77(5)	C_{00F}	C_{00G}	C_{00K}	120.6(5)
C_{007}	N_{005}	C_{00B}	110.6(2)	C_{006}	C_{00H}	C_{00B}	120.3(4)
C_{007}	N_{005}	C_{00E}	109.7(3)	C_{00F}	C_{00H}	C_{006}	118.5(4)
C_{00C}	N_{005}	C_{007}	113.1(3)	C_{00F}	C_{00H}	C_{00B}	121.1(4)
C_{00C}	N_{005}	C_{00B}	107.7(3)	C_{00A}	C_{00I}	C_{00D}	119.8(4)
C_{00C}	N_{005}	C_{00E}	107.8(3)	C_{006}	C_{00J}	C_{00K}	119.8(5)
C_{00E}	N_{005}	C_{00B}	107.8(3)	C_{00J}	C_{00K}	C_{00G}	120.1(5)
C_{00J}	C_{006}	C_{00H}	120.9(4)				

Table S4. The PLQY of $(C_{15}H_{18}N)_2In_{1-x}Sb_xCl_5$

x	PLQY (%)
0.1	107.63
0.2	114.67
0.3	109.82
0.4	108.81
0.5	102.77

Table S5. Crystal data and structure refinement for $(C_{15}H_{18}N)_2InCl_5$ at 170K

Compound	$(C_{15}H_{18}N)_2InCl_5$
Empirical formula	$C_{30}H_{36}Cl_5InN_2$
Formula weight	716.68
Temperature/K	170.15
Crystal system	monoclinic
Space group	*C*2
a/Å	16.1039(15)
b/Å	12.4732(11)
c/Å	8.3236(7)
α/°	90
β/°	103.810(2)
γ/°	90
Volume/Å^3	1623.6(2)
Z	2
ρ_{calc}g/cm^3	1.466
μ/mm^{-1}	1.161
F(000)	728
Crystal size/mm^3	0.12 × 0.11 × 0.1
Radiation	MoK_α (λ = 0.71073)
2Θ range for data collection/°	4.176 to 49.83
Index ranges	$-18 \le h \le 19$, $-14 \le k \le 14$, $-9 \le l \le 9$
Reflections collected	5334
Independent reflections	2612 [R_{int} = 0.0139, R_{sigma} = 0.0259]
Data/restraints/parameters	2612/1/175
Goodness-of-fit on F^2	1.087
Final *R* indexes [I>=2σ (I)]	R_1 = 0.0116, wR_2 = 0.0282
Final *R* indexes [all data]	R_1 = 0.0116, wR_2 = 0.0283
Largest diff. peak/hole / e Å^{-3}	0.13/-0.16
Flack parameter	0.021(7)

3. Supplementary Figures

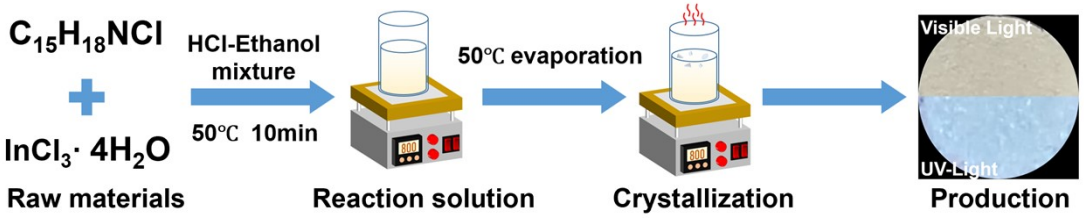

Figure S1. Synthetic route of $(C_{15}H_{18}N)_2InCl_5$.

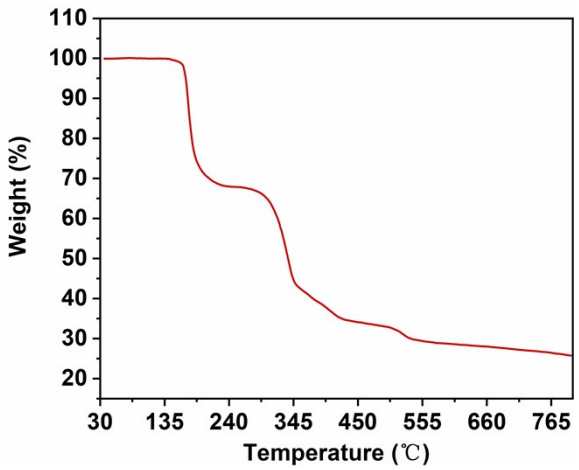

Figure S2. TG spectra of $(C_{15}H_{18}N)_2InCl_5$.

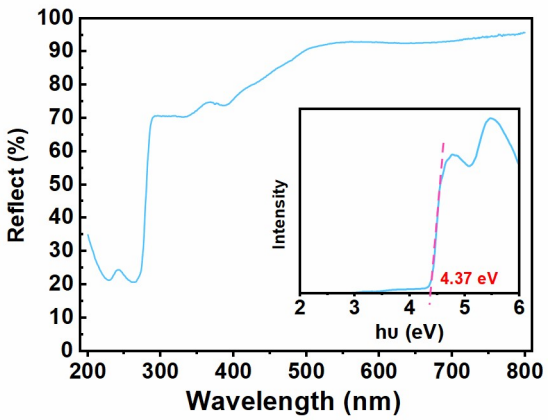

Figure S3. Diffuse Reflectance Spectroscopy spectrum and Tauc plot of $(C_{15}H_{18}N)_2InCl_5$.

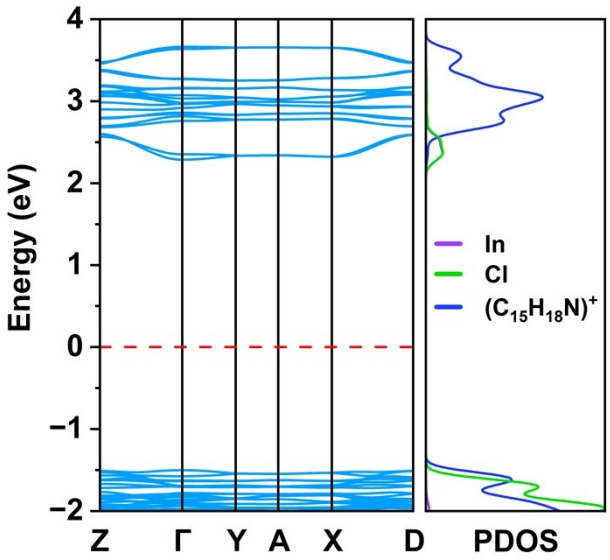

Figure S4. Electronic band structure and PDOS of $(C_{15}H_{18}N)_2InCl_5$.

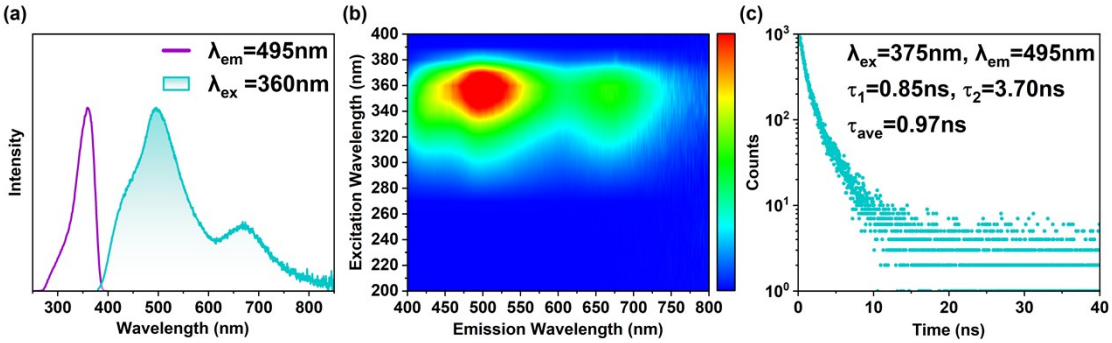

Figure S5. (a) PLE and PL spectra, (b) excitation-dependent emission spectra and (c) PL decay curves of $C_{15}H_{18}NCl$.

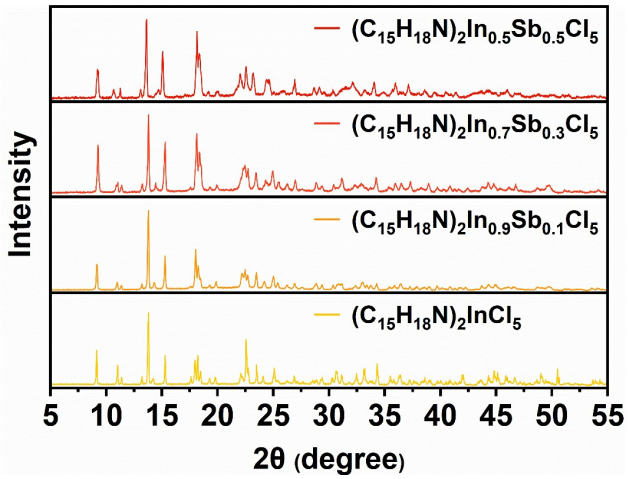

Figure S6. PXRD of $(C_{15}H_{18}N)_2In_{1-x}Sb_xCl_5$.

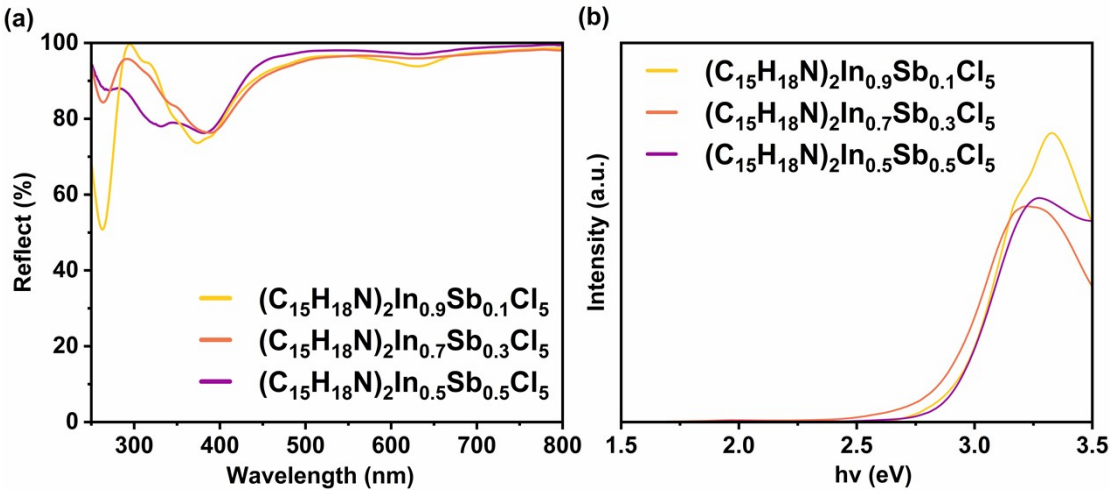

Figure S7. (a) Diffuse Reflectance Spectroscopy spectrum and (b) Tauc plot of $(C_{15}H_{18}N)_2In_{1-x}Sb_xCl_5$.

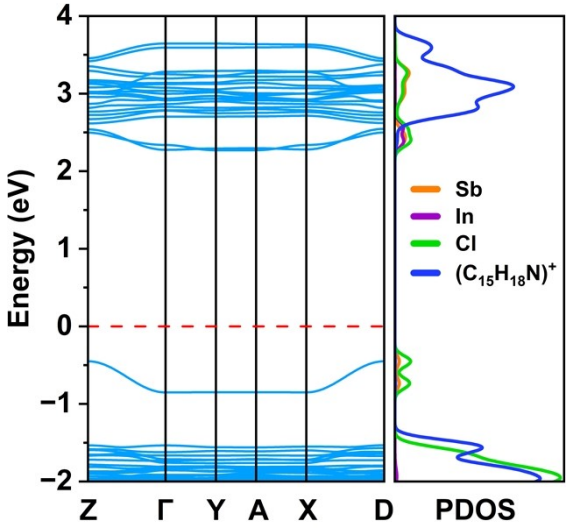

Figure S8. Electronic band structure and PDOS of $(C_{15}H_{18}N)_2In_{1-x}Sb_xCl_5$.

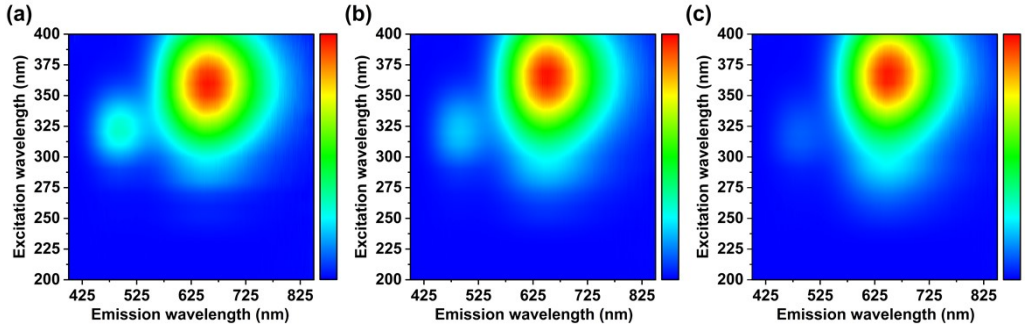

Figure S9. Excitation-dependent emission spectra of (a) $(C_{15}H_{18}N)_2In_{0.9}Sb_{0.1}Cl_5$, (b) $(C_{15}H_{18}N)_2In_{0.7}Sb_{0.3}Cl_5$ and (x) $(C_{15}H_{18}N)_2In_{0.5}Sb_{0.5}Cl_5$.

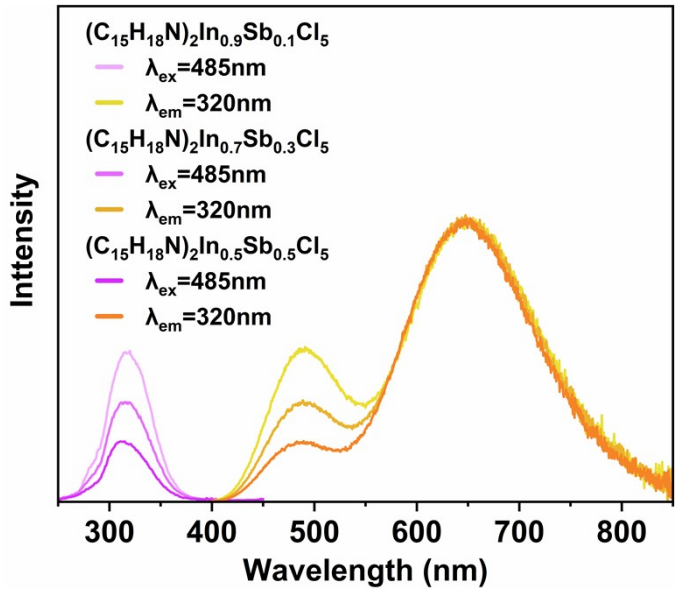

Figure S10. PLE and PL spectra of blue light emission from $(C_{15}H_{18}N)_2In_{1-x}Sb_xCl_5$

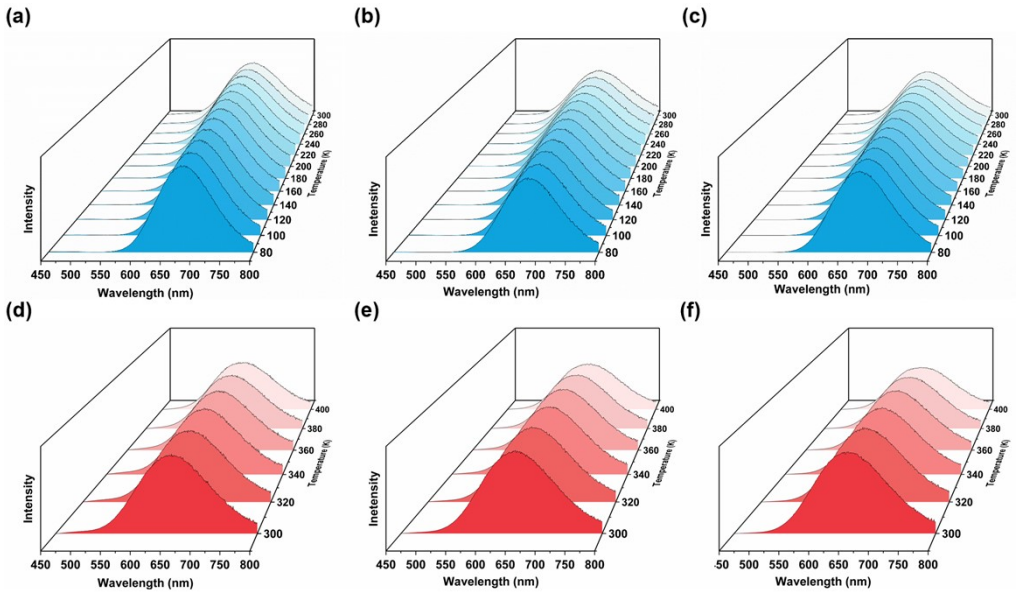

Figure S11. From 80 to 300K, temperature-dependent emission spectra of (a) $(C_{15}H_{18}N)_2In_{0.9}Sb_{0.1}Cl_5$, (b) $(C_{15}H_{18}N)_2In_{0.7}Sb_{0.3}Cl_5$ and (c) $(C_{15}H_{18}N)_2In_{0.5}Sb_{0.5}Cl_5$. From 300 to 400K, temperature-dependent emission spectra of (d) $(C_{15}H_{18}N)_2In_{0.9}Sb_{0.1}Cl_5$, (e) $(C_{15}H_{18}N)_2In_{0.7}Sb_{0.3}Cl_5$ and (f) $(C_{15}H_{18}N)_2In_{0.5}Sb_{0.5}Cl_5$.

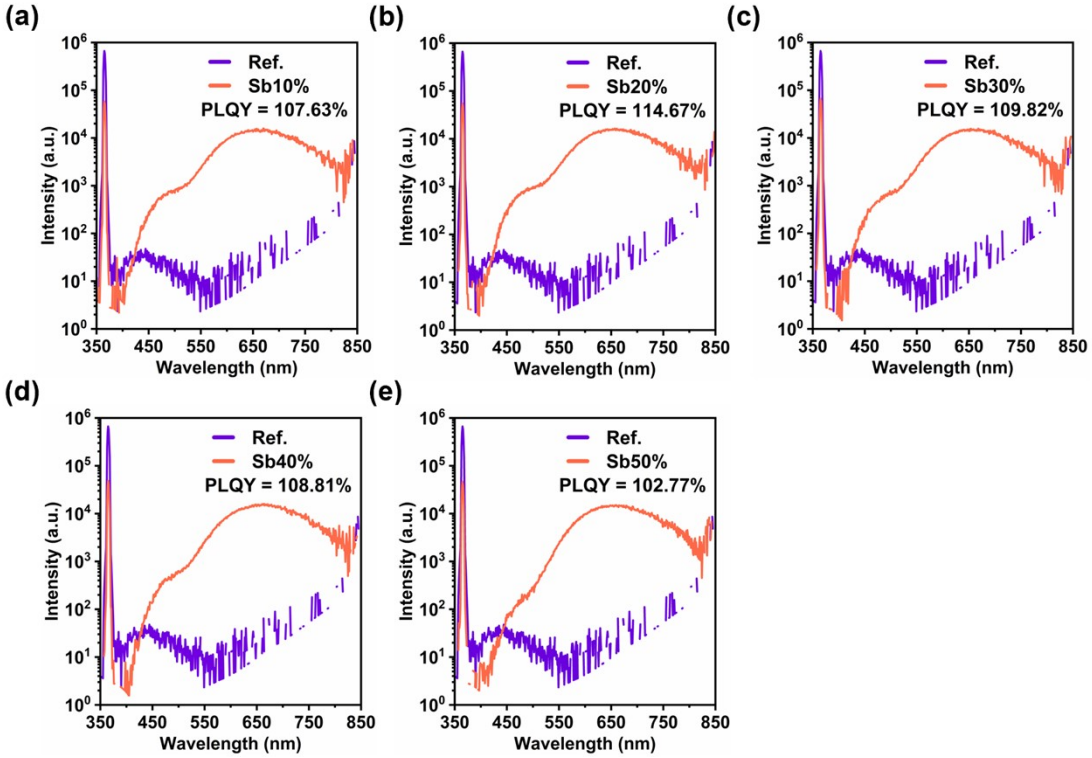

Figure S12. The PLQY of $(C_{15}H_{18}N)_2In_{1-x}Sb_xCl_5$. (a) x = 0.1, (b) x = 0.2, (c) x = 0.3, (d) x = 0.4 and (e) x = 0.5

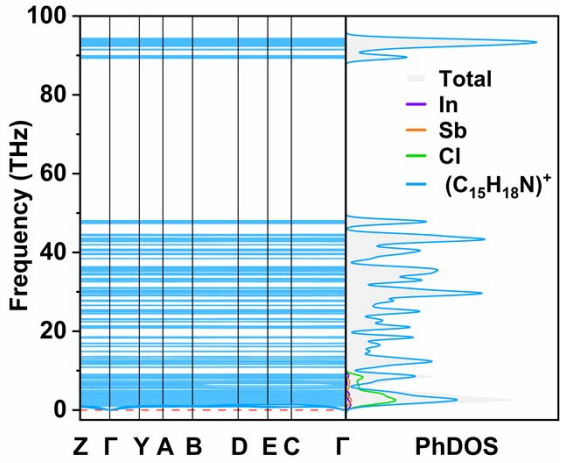

Figure S13. The phonon spectrum and PhDOS of $(C_{15}H_{18}N)_2In_{0.5}Sb_{0.5}Cl_5$.

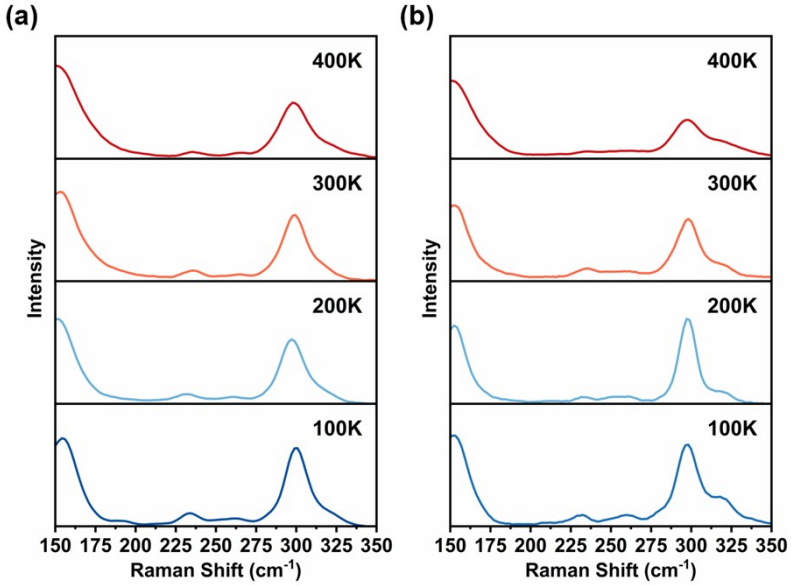

Figure S14. (a) Temperature dependent Raman spectrum of $(C_{15}H_{18}N)_2In_{0.9}Sb_{0.1}Cl_5$, (b) Temperature dependent Raman spectrum of $(C_{15}H_{18}N)_2In_{0.7}Sb_{0.3}Cl_5$

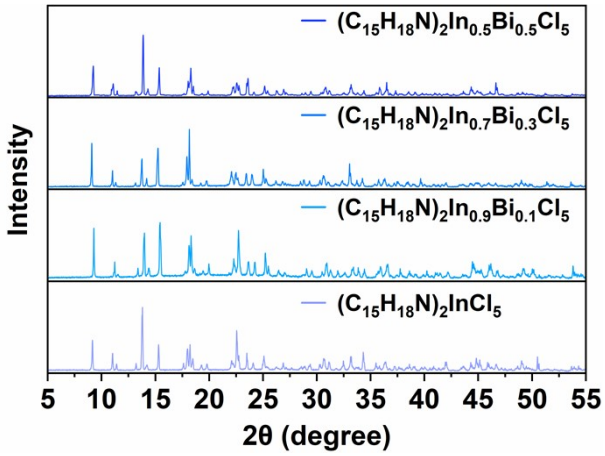

Figure S15. Powder XRD pattern of $(C_{15}H_{18}N)_2In_{1-x}Bi_xCl_5$.

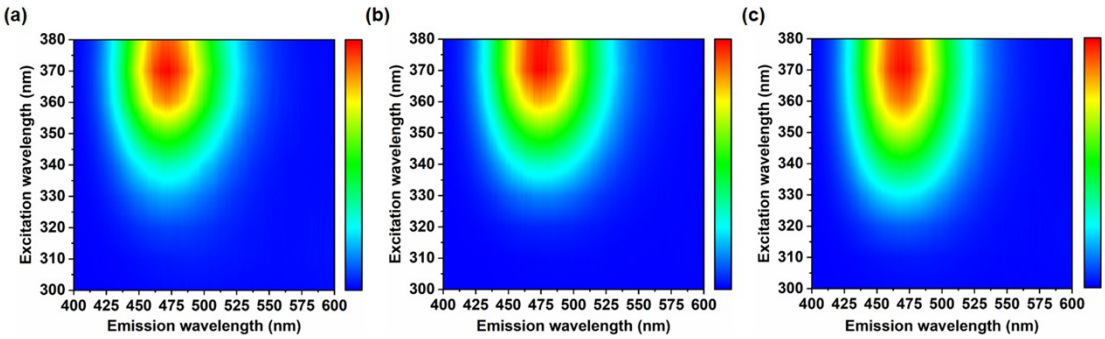

Figure S16. Excitation-dependent emission spectra of (a) $(C_{15}H_{18}N)_2In_{0.9}Bi_{0.1}Cl_5$, (b) $(C_{15}H_{18}N)_2In_{0.7}Bi_{0.3}Cl_5$ and (c) $(C_{15}H_{18}N)_2In_{0.5}Bi_{0.5}Cl_5$

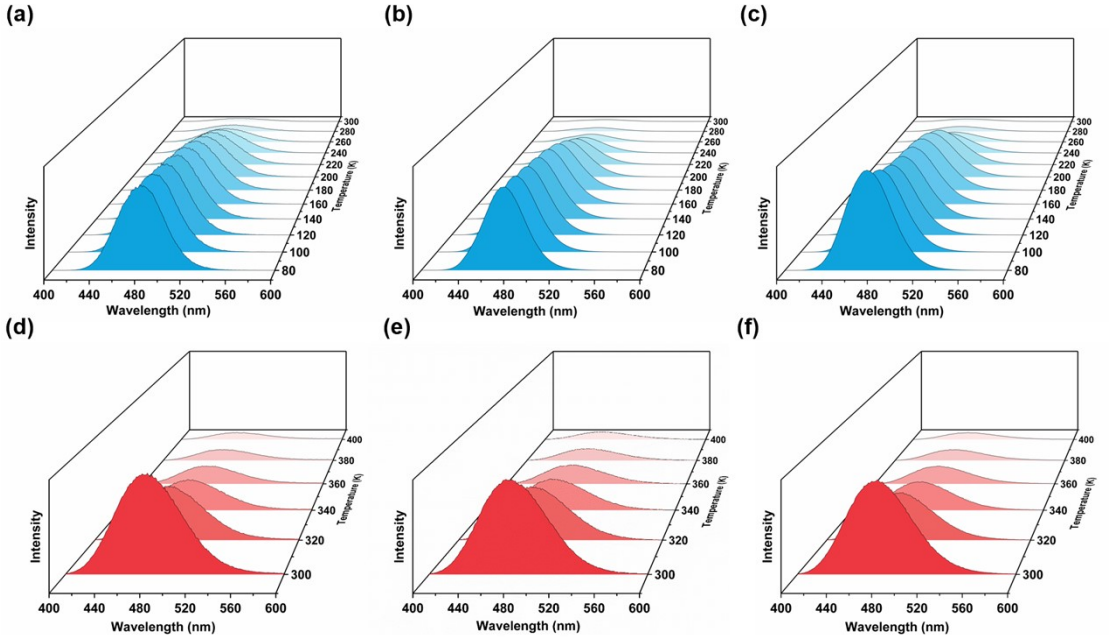

Figure S17. From 80 to 300K, temperature-dependent emission spectra of (a) $(C_{15}H_{18}N)_2In_{0.9}Bi_{0.1}Cl_5$, (b) $(C_{15}H_{18}N)_2In_{0.7}Bi_{0.3}Cl_5$ and (c) $(C_{15}H_{18}N)_2In_{0.5}Bi_{0.5}Cl_5$. From 300 to 400K, temperature-dependent emission spectra of (d) $(C_{15}H_{18}N)_2In_{0.9}Bi_{0.1}Cl_5$, (e) $(C_{15}H_{18}N)_2In_{0.7}Bi_{0.3}Cl_5$ and (f) $(C_{15}H_{18}N)_2In_{0.5}Bi_{0.5}Cl_5$.

References

[1] Kresse, G.; Furthmüller, J., Efficient iterative schemes for ab initio total-energy calculations using a plane-wave basis set. Physical Review B 1996, 54 (16), 11169-11186.

[2] Kresse, G.; Joubert, D., From ultrasoft pseudopotentials to the projector augmented-wave method. Physical Review B 1999, 59 (3), 1758-1775.

[3] Blöchl, P. E., Projector augmented-wave method. Physical Review B 1994, 50 (24), 17953-17979.

[4] Grimme, S.; Antony, J.; Ehrlich, S.; Krieg, H., A consistent and accurate ab initio parametrization of density functional dispersion correction (DFT-D) for the 94 elements H-Pu. The Journal of Chemical Physics 2010, 132 (15).

[5] Togo, A.; Tanaka, I., First principles phonon calculations in materials science. Scripta Materialia 2015, 108, 1-5.